Molecular Orbital and Spectroscopic Studies of Triple Bonds between Transition-Metal Atoms. 1. The d^3–d^3 Mo_2L_6 Compounds (L = OR, NR_2, CH_2R)

Bruce E. Bursten,[1a] F. Albert Cotton,*[1a] Jennifer C. Green,[1b] Elaine A. Seddon,[1b] and George G. Stanley[1a]

Contribution from the Department of Chemistry, Texas A&M University, College Station, Texas 77843, and the Inorganic Chemistry Laboratory, Oxford University, Oxford, England. *Received December 26, 1979*

Abstract: The valence electronic structure of several compounds containing triple bonds between molybdenum atoms has been investigated by using molecular orbital theory and photoelectron spectroscopy (PES). Xα–SW calculations have been performed on $Mo_2(OH)_6$, $Mo_2(NH_2)_6$, $Mo_2(NMe_2)_6$, and $Mo_2(CH_3)_6$, and the projected Xα formalism has been used to determine accurate orbital populations and atomic charges. The calculated transition state ionization potentials agree quite favorably with the He I PE spectra of $Mo_2(OCH_2CMe_3)_6$, $Mo_2(NMe_2)_6$, and $Mo_2(CH_2SiMe_3)_6$. The 7–10-eV binding energy region of $Mo_2(OCH_2CMe_3)_6$ shows three well-resolved bands which are assigned to Mo–Mo π bond, Mo–Mo σ bond, and O lone-pair ionizations, in order of increasing ionization potential. The spectra of the dimethylamido and trimethylsilylmethyl derivatives are more complicated due to the interspersing of metal- and ligand-based ionizations, but they are quite satisfactorily assigned by the calculations. Atomic charge analysis indicates significantly greater ligand-to-metal donation in $Mo_2(CH_3)_6$ than in the alkoxy or amido derivatives. This has been used to explain trends in the structure and reactivity of the compounds. Finally, the calculations are used to dispute the recent proposal that the eclipsed rotational confomer should be preferable to the staggered conformer for small ligands.

Introduction

The study of bonding interactions between transition-metal atoms in their compounds has grown enormously within the past 15 years,[2] with particular interest centered on the chemistry and structure of compounds containing multiple metal–metal bonds. While greatest attention has been devoted to metal–metal quadruple bonds because of their relatively recent discovery among the transition metals, research on M–M triple bonding has recently emerged from its "secondary" status into a large and viable field of its own.[2b] The reaction chemistry and physical properties of these systems are proving to be most unusual,[2,3] and active synthetic programs are underway in several major research groups throughout the inorganic community. Despite all the synthetic and structural interest, however, the investigation of the electronic structures of these compounds has been somewhat neglected. A more precise understanding of the electronic factors involved in these systems would allow much greater insight into the origins of the various physical properties and reaction chemistry.

There are two general classes of metal-to-metal triple bonding which lie, electronically speaking, on either side of the M–M quadruple bond. Both are composed of one σ- and two π-type metal–metal bonds which constitute a bond order of three. The first broad category of M–M triple bonding is that in which these are the only electrons shared by the metal atoms; there are two electrons less than those needed to reach the d^4–d^4 electronic configuration of a quadruple bond (Figure 1). The δ component of the quadruple bond is totally absent, leaving only a d^3–d^3 triple bond. The second category of triple M–M bonds are those which may be denoted d^5–d^5, with the δ bond being abolished by the presence of two electrons in the δ* orbital. It is the former class of compounds which are the subject of this paper; the d^5–d^5 triply bonded compounds will be the subject of a later publication.

The most widely studied class of d^3–d^3 triple-bonded metal dimers have the general formula M_2L_6,[2,3] where M = Mo and W and L = R (alkyl), NR_2, and OR. $Mo_2(CH_2SiMe_3)_6$, the first compound in this series, was discovered by Wilkinson and co-workers in 1971 as a product formed in the reaction of $MoCl_5$ with 5 equiv of $LiCH_2SiMe_3$.[4] It was shown to have a rather short Mo–Mo bond distance of 2.167 Å[5] and a staggered ethane-like conformation. The broad interest in, and systematic development of, this new class of metal dimers did not take place, however, until 1975 with the synthesis and characterization of $Mo_2(NMe_2)_6$ and $W_2(NMe_2)_6$ by Chisholm and co-workers.[6,7] Since then a large number of M_2L_6 compounds have been prepared and studied.[2]

The metal atoms in these M_2L_6 compounds possess only a 12-electron valence-shell configuration which means that they are very electronically unsaturated. Not too surprisingly then, these compounds exhibit extensive substitution,[8,9] insertion,[10–12] and addition[13–16] chemistries. $Mo_2(OR)_6$ compounds, for example, react reversibly with donor ligands such as phosphines or amines yielding $Mo_2(OR)_6L_2$ adducts.[13] CO_2 easily inserts into M_2L_6 (L = OR, NR_2) metal–ligand bonds forming $Me(O_2CL)_2L_4$,[12] $M_2(O_2CL)_4L_2$,[10] or $M_2(O_2CL)_6$[10] complexes, although such insertion reactions are not observed for M–C bonds. Most of these insertion and addition reactions result in little or no change in the M–M bond length, probably because the 12-electron configurations and coordinative unsaturation allow the acquisition of more electrons without effect upon the M–M bonding.

(1) (a) Texas A&M University. (b) Oxford University.
(2) (a) Cotton, F. A. *Acc. Chem. Res.* **1978**, *11*, 225. (b) Chisholm, M. H.; Cotton, F. A. *Ibid.* **1978**, *11*, 356.
(3) Chisholm, M. H.; Extine, M.; Reichert, W. *Adv. Chem. Ser.* **1976**, *No. 150*, 273.
(4) Huq, F.; Mowat, W.; Shorthand, A.; Skapski, A. C.; Wilkinson, G. *Chem. Commun.* **1971**, 1079.
(5) Bond distances will be given with the estimated standard deviation in the last digit for that distance in parentheses following the number. When no esd is given, it was either unavailable (as in this case) or not pertinent to the discussion.
(6) Chisholm, M. H.; Cotton, F. A.; Frenz, B. A.; Reichert, W. W.; Shive, L. W.; Stults, B. R. *J. Am. Chem. Soc.* **1976**, *98*, 4469.
(7) Chisholm, M. H.; Cotton, F. A.; Extine, M.; Stults, B. R. *J. Am. Chem. Soc.* **1976**, *98*, 4477.
(8) Chisholm, M. H.; Cotton, F. A.; Extine, M.; Millar, M.; Stults, B. R. *Inorg. Chem.* **1976**, *15*, 2244.
(9) Chisholm, M. H.; Cotton, F. A.; Extine, M. W.; Millar, M.; Stults, B. R. *Inorg. Chem.* **1977**, *16*, 320.
(10) Chisholm, M. H.; Cotton, F. A.; Extine, M.; Stults, B. R. *Inorg. Chem.* **1977**, *16*, 603.
(11) Chisholm, M. H.; Extine, M. W. *J. Am. Chem. Soc.* **1977**, *99*, 782, 792.
(12) Chisholm, M. H.; Cotton, F. A.; Extine, M. W.; Reichert, W. W. *J. Am. Chem. Soc.* **1978**, *100*, 1727.
(13) Chisholm, M. H.; Cotton, F. A.; Extine, M. W.; Reichert, W. W. *J. Am. Chem. Soc.* **1978**, *100*, 153.
(14) Chisholm, M. H.; Cotton, F. A.; Extine, M. W.; Kelly, R. L. *J. Am. Chem. Soc.* **1978**, *100*, 2256.
(15) Chisholm, M. H.; Cotton, F. A.; Extine, M. W.; Kelly, R. L. *Inorg. Chem.* **1979**, *18*, 116.
(16) Chisholm, M. H.; Cotton, F. A.; Extine, M. W.; Kelly, R. L. *J. Am. Chem. Soc.* **1978**, *100*, 3354.

0002-7863/80/1502-4579$01.00/0

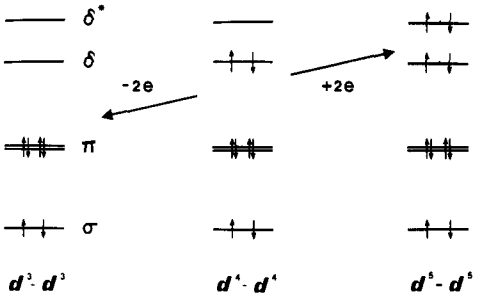

Figure 1. A qualitative MO diagram illustrating the two general types of M–M triple bonds formed by the subtraction (d^3–d^3) or addition (d^5–d^5) of two electrons to the d^4–d^4 M–M quadruple bond.

The short Mo–Mo bond distances and diamagnetism of all the compounds studied and the absence of bridging ligands all point clearly to the existence of strong metal–metal bonding. The qualitative view that the metal–metal bond is composed of one σ bond, formed by the overlap of metal d_{z^2} orbitals, and two π components made up of d_{xz} and d_{yz} metal orbitals was confirmed by Xα–SW calculations on $Mo_2(OH)_6$, $Mo_2(NH_2)_6$, and $Mo_2(NMe_2)_6$ reported by us in a preliminary communication in 1977.[17] Subsequent Hartree–Fock[18] and extended Hückel[19] calculations have arrived at similar electronic structures. While there have been no fundamental disagreements thus far as to the general electronic structure of these M_2L_6 systems, Hoffmann and Albright recently argued[19] that empirical extended Hückel calculations on several M_2L_6 systems (L = H, Cl, and CO) imply substantial mixing of the metal π (d_{xz}, d_{yz}), δ (d_{xy}, $d_{x^2-y^2}$), and 5p orbitals in the M–M π-bonding levels, resulting in directed hybrid orbitals which favor an eclipsed ligand conformation, whereas the $\sigma^2\pi^4$ configuration carries the implication that there is no barrier to rotation. It was suggested[19] that with small enough ligands an eclipsed structure might actually be found. This question will be further explored in this paper by using the projected Xα (PXα) method[20] to obtain LCAO molecular orbitals from the numerical Xα orbitals. This technique facilitates a detailed examination of the more accurate Xα results to see whether any such hybridization is actually occurring.

Calculations on $Mo_2(OH)_6$, $Mo_2(NH_2)_6$, $Mo_2(NMe_2)_6$, and $Mo_2(CH_3)_6$ are reported in detail here in an attempt to quantify the metal–metal and metal–ligand bonding, as well as the synergistic effects that each one has upon the other. Comparisons between the Xα–SW calculations and photoelectron spectra will be presented, and it will be shown that excellent qualitative, and in some cases quantitative, agreement is found. Finally, the results of these calculations will be used to explain some of the reactivity and bonding patterns known for the compounds.

Procedures

General. A revised double-precision SCF-Xα–SW program package by M. Cook (Harvard) and B. E. Bursten and G. G. Stanley (Texas A&M) was used on an Amdahl 470 V/6 computing system. The α values were taken from the α_{HF} tabulation of Schwarz[21] except for hydrogen, for which α was chosen to be 0.777 25. A valence-electron weighted average of the atomic α values was used for the inter- and outer-sphere regions. Overlapping atomic sphere radii were taken as 89% of the atomic number radii calculated by the molecular superposition program.[22] All radii so used were found to be satisfactory in the sense of giving virial ratios, $-2T/V$, of 1.000 ± 0.001 for all calculations and were not further optimized. The outer-sphere radius was made tangential to the outermost atomic sphere in each calculation. Ionization potentials were calculated by using Slater's transition-state formalism[23] which takes account of second-order relaxation effects. The basis sets used for atomic orbital projection consisted of Slater-type orbitals (STO's) optimized to the atomic calculations.[24] Contracted double-ζ functions were used for the Mo 4d and the C, N, and O 2p orbitals; single-ζ functions were used for the remaining valence AO's, including Mo 5s and 5p. The integration grid used for the projection consisted of 25 quadrature points in r, nine in θ, and nine in ϕ.

$Mo_2(OH)_6$. The bond distances and angles for the calculation on $Mo_2(OH)_6$ were taken from the crystal structure[25] of $Mo_2(OCH_2CMe_3)_6$ and averaged to conform to idealized D_{3d} symmetry. The bond distances and angles used are Mo–Mo = 2.222 Å, Mo–O = 1.88 Å, O–H = 0.958 Å, Mo–Mo–O = 104°, and Mo–O–H = 109°. The initial molecular potential for $Mo_2(OH)_6$ was constructed from a superposition of Herman–Skillman[26] atomic potentials for $Mo^{1.5+}$ and $O^{0.5-}$ with the hydrogen atomic potential generated from the exact H 1s radial function. The sphere radii used were as follows: Mo, r = 2.4170 au; O, r = 1.7221 au; H, r = 1.0874 au. The outer-sphere radius equals 6.2650 au. The D_{3d} symmetry-adapted linear combinations of atomic orbitals included partial waves through l = 2 on the molybdenum atoms, through l = 1 on the oxygen atoms, through l = 0 on the hydrogen atoms, and through l = 5 on the outer sphere.

The SCF calculations were started by using a 5% mixing of the new potential into the old to generate the starting potential for the next iteration. The mixing was gradually raised to a maximum of ~25%. The SCF calculation required approximately 30 iterations to reach convergence which was assumed when the maximum shift in the potential from one iteration to the next was less than 0.0010 Ry. Each iteration required about 8 s of execution time.

The energy levels previously reported[17] for $Mo_2(OH)_6$ are slightly in error due to a mistake found in the symmetry functions for the e_u representation. Furthermore, the absolute positions of the levels are now somewhat different as the present calculations were reconverged using a smaller convergence criterion and double-precision programs. No significant differences between the two calculations were apparent, however.

$Mo_2(NH_2)_6$. The bond distances and angles for $Mo_2(NH_2)_6$ were taken from the crystal structure[6] of $Mo_2(NMe_2)_6$ and averaged to conform to idealized D_{3d} symmetry. The bond distances and angles used are as follows: Mo–Mo = 2.214 Å, Mo–N = 1.980 Å, N–H = 0.975 Å, Mo–Mo–N = 103.7°, Mo–N–H1 = 116.3°, Mo–N–H2 = 133.4°, and H–N–H = 110.2°. The coordinate system for this calculation (and, by analogy, all of the others) is shown below.

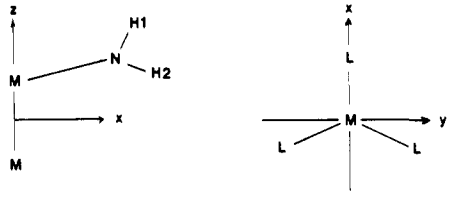

The initial molecular potential for $Mo_2(NH_2)_6$ was constructed from $Mo^{1.5+}$ and $N^{0.5-}$ Herman–Skillman atomic potentials and hydrogen 1s radial functions. The sphere radii used are as follows: Mo, r = 2.5053 au; N, r = 1.7093 au; H1 and H_2, r = 1.1241 au. The outer-sphere radius was 6.9848 au. The D_{3d} SALC's were the same as for $Mo_2(OH)_6$.

As before, a 5% mixing of the new potential into the old to generate the starting potential for the next iteration was gradually increased to a maximum value of ~25%. The SCF calculation required approximately 30 iterations to reach convergence, with a typical iteration requiring about 9 s of execution time.

$Mo_2(NMe_2)_6$. The bond distances and angles for $Mo_2(NMe_2)_6$ were taken from the crystal structure[6] on $Mo_2(NMe_2)_6$ and idealized to conform with D_{3d} symmetry. The bond distances and angles used are as follows: Mo–Mo = 2.214 Å, Mo–N = 1.980 Å, N–C = 1.470 Å, C–H = 0.975 Å, Mo–Mo–N = 103.7°, Mo–N–C1 = 116.3°, Mo–N–C2 = 113.4°, and N–C–H angles = 115.0°. The initial molecular potential was constructed by using $Mo^{1.5+}$, $N^{0.5-}$, and CO atomic potentials and H 1s radial functions. The sphere radii used are as follows: Mo, r = 2.4921 au; N, r = 1.6952 au; C, r = 1.6410; H, r = 1.1828. The outer-sphere radius equals 9.4573 au. Approximately 60 iterations were required to convergence with a typical iteration taking 100 s of execution time.

(17) Cotton, F. A.; Stanley, G. G.; Kalbacher, B. J.; Green, J. C.; Seddon, E.; Chisholm, M. H. *Proc. Natl. Acad. Sci. U.S.A.* **1977**, *74*, 3109.
(18) Hillier, I. H.; Garner, C. D.; Mitcheson, G. R. *Chem. Commun.* **1978**, 204.
(19) Albright, T. A.; Hoffmann, R. *J. Am. Chem. Soc.* **1978**, *100*, 7736.
(20) Bursten, B. E.; Fenske, R. F. *J. Chem. Phys.* **1977**, *67*, 3138.
(21) Schwarz, K. *Phys. Rev. B* **1972**, *5*, 2466.
(22) Norman, J. G. *Mol. Phys.* **1976**, *31*, 1191.
(23) Slater, J. C. "Quantum Theory of Molecules and Solids: The Self-Consistent Field for Molecules and Solids"; McGraw-Hill: New York, 1974; Vol. 4.
(24) Bursten, B. E.; Jensen, J. R.; Fenske, R. F. *J. Chem. Phys.* **1978**, *68*, 3320.
(25) Chisholm, M. H.; Cotton, F. A.; Murillo, C. A.; Reichert, W. W. *Inorg. Chem.* **1977**, *16*, 1801.
(26) Herman, F.; Skillman, S. "Atomic Structure Calculations"; Prentice-Hall: Englewood, Cliffs, NJ, 1963.

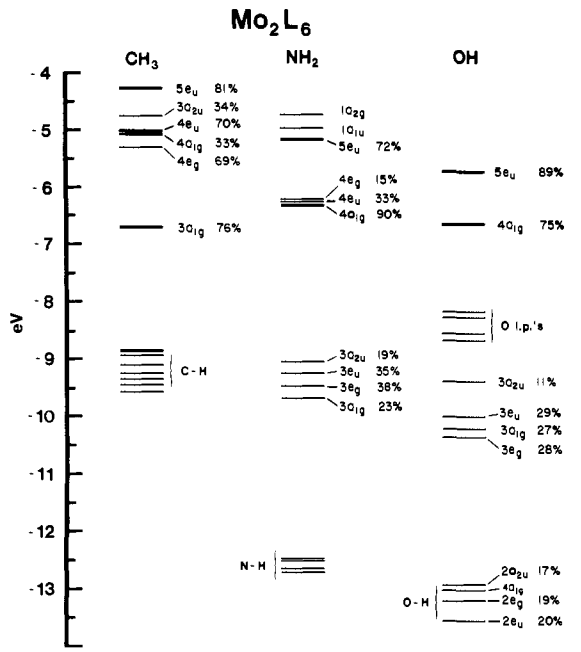

Figure 2. Xα–SW energy level diagrams for $Mo_2(OH)_6$, $Mo_2(NH_2)_6$, and $Mo_2(CH_3)_6$. Only the occupied upper valence orbitals are shown. Percent characters are from LCAO projection on each molecule and represent the molybdenum contribution to that orbital.

$Mo_2(CH_3)_6$. The bond distances and angles for $Mo_2(CH_3)_6$ were taken from the crystal structure[4] of $Mo(CH_2SiMe_3)_6$ and idealized to conform to D_{3d} symmetry. The bond distances and angles used are as follows: Mo–Mo = 2.167 Å, Mo–C = 2.131 Å, C–H = 1.00 Å, Mo–Mo–C = 100.6°, and Mo–C–H = 115.0°. The initial molecular potential was constructed from $Mo^{1.5+}$ and $C^{0.5-}$ atomic potentials and H 1s radial functions. The sphere radii used are as follows: Mo, r = 2.6121 au; C, r = 1.7416 au; H, r = 1.2022 au. The outer-sphere radius equals 8.1401 au. Approximately 45 iterations were required to reach convergence with a typical iteration taking 14 s of execution time.

Experimental Details. Compounds were prepared and characterized as described elsewhere.[4,7,27] He I and He II photoelectron spectra were obtained by using a Perkin-Elmer PS 16/18 photoelectron spectrometer fitted with a Helectros lamp. To obtain sufficient intensity (about 400 c/s), we heated the compounds to the following temperatures: 60–70 °C for $Mo_2(OCH_2CMe_3)_6$; 90–100 °C for $Mo_2(NMe_2)_6$; 115–135 °C for $Mo_2(CH_2SiMe_3)_6$.

Results and Discussion

$Mo_2(OH)_6$. The results of the Xα–SW calculation of the model compound, $Mo_2(OH)_6$, are presented in Figure 2. The valence orbitals of all three model systems $Mo_2(OH)_6$, $Mo_2(NH_2)_6$, and $Mo_2(CH_3)_6$ have been projected onto an AO basis, thus eliminating the atomic-, inter-, and outer-sphere charge ambiguities as well as giving a more useful LCAO decomposition of the atomic characters. The MO contributions discussed for $Mo_2(OH)_6$, $Mo_2(NH_2)_6$, and $Mo_2(CH_3)_6$ will be those from the LCAO projections unless otherwise noted. The projected Xα (PXα) orbital characters and orbital energies for $Mo_2(OH)_6$ are listed in Table I.

The upper valence orbitals in $Mo_2(OH)_6$ can be grouped very naturally into four categories: (1) the Mo–Mo bonding orbitals; (2) oxygen lone-pair levels, (3) Mo–O σ-bonding MO's, and (4) O–H and Mo–O π-bonding orbitals. The highest occupied molecular orbital (HOMO) is the $5e_u$ level which has 89% Mo character and is mainly Mo–Mo π bonding as demonstrated in the contour plot of the $5e_u$ orbital wave function[28] in Figure 3.

Table I. Energies and Percent Characters of the Highest Occupied Orbitals of $Mo_2(OH)_6$

		Mulliken percent contributions						
		Mo[a,b]					O	
level	ε, eV	σ	π	δ	5s	5p	2s	2p
$5e_u$	−5.75		80.8	3.4		4.6	2.5	6.6
$4a_{1g}$	−6.66	63.2			11.8			19.2
$1a_{2g}$	−8.19							99.1
$1a_{1u}$	−8.30							99.1
$4e_g$	−8.59		2.8					96.2
$4e_u$	−8.72		2.8					96.2
$3a_{2u}$	−9.42	11.2					0.9	86.5
$3e_u$	−10.02			28.6				71.0
$3a_{1g}$	−10.23	27.2						71.8
$3e_g$	−10.39			28.6			1.6	69.8
$2a_{2u}$	−12.95				17.4		5.4	55.8
$2a_{1g}$	−13.05				5.3		7.2	64.0
$2e_g$	−13.23		7.0	5.0		7.1	4.0	54.0
$2e_u$	−13.59		14.2	5.9			4.5	47.8

[a] $\sigma = 4d_{z^2}$; $\pi = 4d_{xz}, 4d_{yz}$; $\delta = 4d_{xy}, 4d_{x^2-y^2}$. [b] Spaces indicate contributions less than 0.4%. Hydrogen 1s contributions are not listed but are the difference between the sum of the contributions shown and 100%.

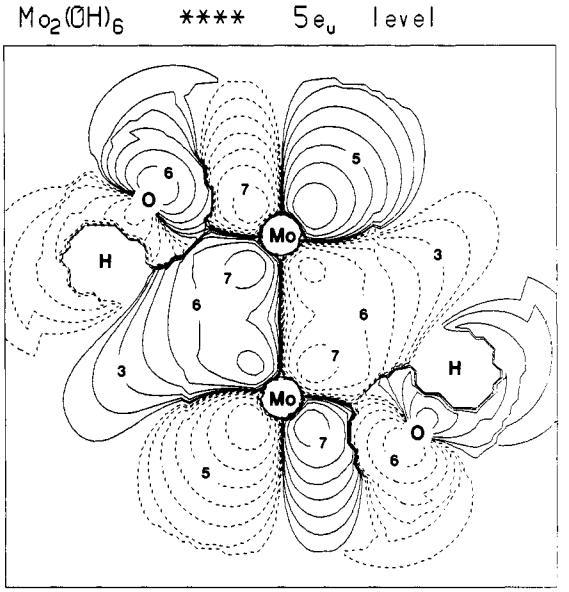

Figure 3. Contour plot of the $5e_u$ orbital wave function of $Mo_2(OH)_6$. Dashed lines indicate negative contour values. Contour values are as follows: ±1 = 0.0025; ±2 = 0.005; ±3 = 0.010; ±4 = 0.020; ±5 = 0.040; ±6 = 0.080; and ±7 = 0.160 electrons/Å^3. These contour values are used in all the contour plots shown.

As can be seen in the contour plot, there is also Mo–O π*-antibonding character present. The two oxygen atoms in the plot have in-plane[29] Mo–O π* interactions while the other four ligands make Mo–O π* contributions via their out-of-plane 2p AO's. A slight difference in the lobal extensions of the Mo π orbitals is also evident. This arises from both the influence of the oxygen atoms and slight mixing of molybdenum δ* and 5p character with the Mo–Mo π bond.

The other principal Mo–Mo bonding level is the $4a_{1g}$ which is strongly Mo–Mo σ bonding, but Mo–O antibonding (Figure 4). The 75% Mo contribution to the $4a_{1g}$ level is a composite of 63% $4d_{z^2}$ and 12% 5s characters. The 5s–$4d_{z^2}$ interaction between the metal atoms is bonding, thus contributing to the metal–metal bond and reducing the Mo–O antibonding interactions.

The next set of orbitals, clustered between −8.0 and −8.7 eV, represents the noninteracting, out-of-plane oxygen lone-pair levels.

(27) Chisholm, M. H.; Reichert, W.; Cotton, F. A.; Murillo, C. A. *J. Am. Chem. Soc.* **1977**, *99*, 1652.

(28) The discontinuities in the plots are due to improper matching conditions at the atomic- and outer-sphere boundaries. They have no physical significance or effect on the calculations except to make the contour plots look "jagged". By adding more l waves in the symmetry basis functions the boundary conditions become better matched, but the cost of the calculation goes up, and no real difference in the energy levels is seen.

(29) "In-plane" refers to the D_{3d} dihedral mirror planes which pass through the ligands and Mo–Mo bond. The contour plots are slicing through the molecule coincident with one of the mirror planes.

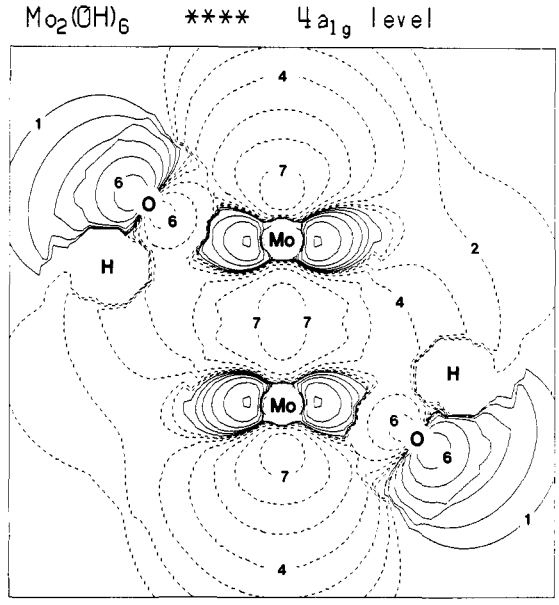

Figure 4. Contour plot of the $4a_{1g}$ orbital of $Mo_2(OH)_6$.

These MO's are virtually pure oxygen in character, with only slight Mo $d\pi$ contributions occurring in the $4e_u$ and $4e_g$ orbitals. The $3a_{2u}$ through $3e_g$ MO's, which are below the lone-pair levels, are strongly Mo–O σ bonding and represent the main M–L bonding orbitals. The $3a_{2u}$ MO is composed of molybdenum $4d_{z^2}$ orbitals which are engaged in Mo–O bonding through the d_{z^2} "doughnuts". The Mo–Mo interaction is antibonding (σ^*), accounting for the destabilization of the $3a_{2u}$ level from the other M–L bonding orbitals. The $3a_{1g}$ MO is the metal–ligand bonding counterpart of the $4a_{1g}$ level. It is Mo–Mo and Mo–O bonding but with a Mo contribution of only 27% is classed primarily as a M–L bonding orbital. The $3e_u$ and $3e_g$ orbitals are also Mo–O bonding and are pure Mo δ in nature. The $3e_g$ level is metal–metal δ bonding and is therefore at lower energy than the $3e_u$ which is δ^*. The separation is fairly small, however, attesting to the dominance of the Mo–O bonding and the small effect of the δ or δ^* Mo–Mo interactions. While the lower set of orbitals in Figure 2 are mainly O–H bonding, they also have significant Mo–O bonding interactions, although not as strong as those just discussed. The $2e_g$ and $2e_u$ orbitals are particularly interesting since they have in-plane Mo–O π bonding mixed in with the O–H bonding. The δ mixing present in each orbital favors the Mo–O bonding, and in the case of the $2e_g$ level, which has proportionately more δ character, the Mo–Mo π^* interaction is reduced.

The presence of Mo–O π bonding, in addition to the expected σ bonds, confirms an earlier original proposal[25] that π bonding is probably present, offering one explanation for the rather short Mo–O bond distance of 1.88 Å. It is interesting to note, however, that the metal–ligand π bonding does not arise from the out-of-plane oxygen lone pairs, but from the O–H (or O–R) bonding orbitals mixing with the metal π orbitals.

The calculated ionization potentials (IP's) for $Mo_2(OH)_6$ are listed in Table II. They follow the same general trend shown in the energy level diagram in Figure 2. We will only be concerned with the relative placement of the orbitals, and not their absolute positions; the choice of atomic- and outer-sphere radii can cause approximately uniform shifts in the energy levels but makes very little difference in the atomic contributions to the orbitals or their relative spacings. The calculation predicts that there should be two peaks separated by about 0.8 eV, attributed to the Mo–Mo π and σ levels, followed by a band $\sim$1.2 eV higher in energy composed of ionizations from four oxygen lone-pair orbitals. Theoretical He I photoionization cross sections for these six orbitals were calculated by using the scattered-wave formalism developed by Davenport.[30] In order to generate a simulated PE spectrum

(30) Davenport, J. W. *Phys. Rev. Lett.* **1976**, *36*, 945.

Table II. Calculated Transition State Ionization Potentials for $Mo_2(CH_3)_6$, $Mo_2(NH_2)_6$, and $Mo_2(OH)_6$

$Mo_2(CH_3)_6$		$Mo_2(NH_2)_6$		$Mo_2(OH)_6$	
level	IP[a]	level	IP	level	IP
$5e_u$	6.21	$1a_{2g}$	7.05	$5e_u$	8.71
$3a_{2u}$	6.80	$1a_{1u}$	(7.3)	$4a_{1g}$	9.54
$4a_{1g}$	7.07	$5e_u$	7.62	$1a_{2g}$	10.77
$4e_u$	7.45	$4e_g$	8.42	$1a_{1u}$	(10.9)
$4e_g$	7.50	$4e_u$	8.62	$4e_g$	11.15
$3a_{1g}$	9.45	$4a_{1g}$	9.01	$4e_u$	11.28
		$3a_{2u}$	11.45	$3a_{2u}$	12.02
		$3e_u$	(11.7)		
		$3e_g$	(11.9)		
		$3a_{1g}$	12.13		

[a] Energies are in eV. Values in parentheses are estimated from nearby ionizations and should be accurate to within 0.1 eV.

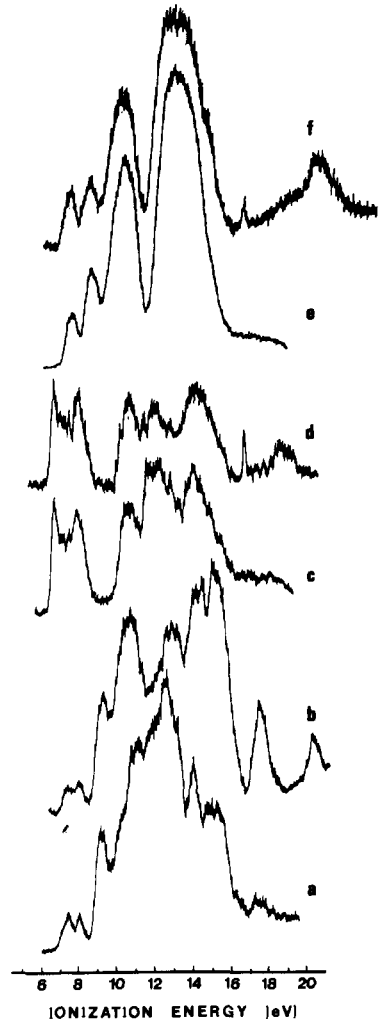

Figure 5. The 6–20-eV photoelectron spectra of compounds containing triple Mo–Mo bonds: (a) He I and (b) He II for $Mo_2(OCH_2CMe_3)_6$; (c) He I and (d) He II for $Mo_2(NMe_2)_6$; (e) He I and (f) He II for $Mo_2(CH_2SiMe_3)_6$.

for $Mo_2(OH)_6$, we have assumed that each ionization has a symmetric Gaussian band shape; the relative intensities and assumed bandwidths at half-height are summarized in Table III. In Figure 5, the experimental He I PE spectrum for $Mo_2(OCH_3CMe_3)_6$ is compared to the simulated spectrum, which has been shifted upward in energy by 1.31 eV to match the first theoretical peak with the first experimental peak. The full range (6–20 eV) He I and He II PE spectra are shown in Figure 6a,b.

The agreement between the theoretical and experimental spectra is quite good. The experimental vertical IP's are 7.40, 8.02, and 9.28 eV. The calculated spacing between the first two levels, 0.83

Table III. Calculated Relative Intensities and Assumed Bandwidths for the First Six Ionizations of $Mo_2(OH)_6$

level	ionization potential,[a] eV	rel intensity	bandwidth,[b] eV
$5e_u$	7.40	2.99	0.8
$4a_{1g}$	8.23	1.00	0.4
$1a_{2g}$	9.46	0.50	0.4
$1a_{1u}$	9.56	0.40	0.4
$4e_g$	9.84	2.63	0.6
$4e_u$	9.97	2.18	0.6

[a] The ionization potentials have been shifted by 1.31 eV to match the $5e_u$ ionization to the lowest experimental band. [b] Full width at half-maximum for symmetric Gaussian peaks.

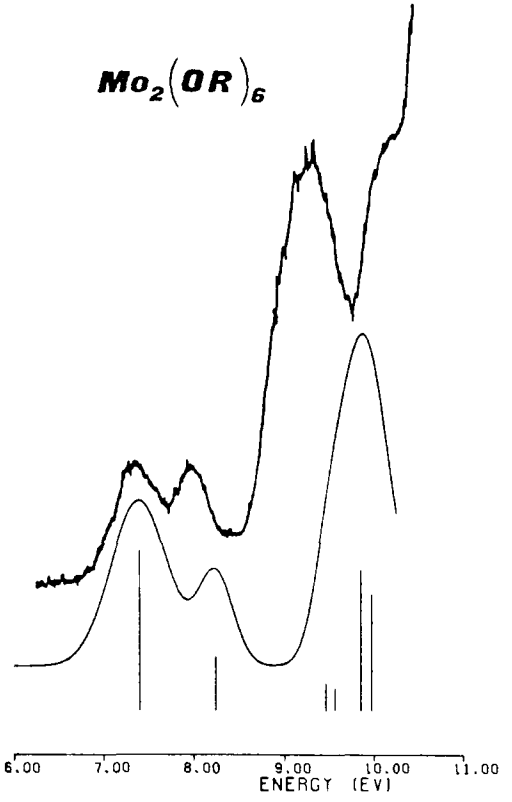

Figure 6. Experimental He I photoelectron spectrum (top) of $Mo_2(OCH_2CMe_3)_6$ and the theoretically generated He I spectrum (bottom) for the model system $Mo_2(OH)_6$. The calculated values were shifted by 1.30 eV in order to match the first experimental and theoretical peaks. The heights of the vertical lines represent relative intensities of the ionizations.

eV, is about 0.2 eV larger than the experimental separation. Although the calculated position of the oxygen lone-pair ionization appears to be too high in energy by ~0.9 eV, we feel that this is largely due to the inductive effect of the CH_2CMe_3 groups. The energetic effects of approximating alkyl groups by hydrogen atoms is seen in our calculations on $Mo_2(NR_2)$ compounds; the replacement of NH_2 by NMe_2 causes an upward shift of ~0.8 eV in the energy of the nitrogen lone-pair ionizations (vide infra). The calculated intensities are quite reasonable as well, although it would appear that the cross section of the $5e_u$ ionization has been overestimated.

We believe that the electronic structure of $Mo_2(OR)_6$ compounds is well represented by the Xα–SW results on the model system $Mo_2(OH)_6$. The various types of MO's are well separated and defined in their function, the metal–metal bonding π and σ levels being the highest in energy, followed by the more electronegative oxygen lone pairs, Mo–O σ-bonding orbitals, and the O–H and Mo–O π-bonding levels. It will next be seen that as the OR groups are replaced by the less electronegative amide and alkyl ligands, this picture will change dramatically and become less simple.

Table IV. Energies and Percent Characters of the Highest Occupied Orbitals of $Mo_2(NH_2)_6$

		Mulliken percent contributions						
		Mo[a,b]					N	
level	ϵ, eV	σ	π	δ	5s	5p	2s	2p
$1a_{2g}$	−4.75							100.0
$1a_{1u}$	−4.99							100.0
$5e_u$	−5.18		62.8			9.4	0.6	23.6
$4e_g$	−6.23		6.7	7.8			2.2	82.7
$4e_u$	−6.28		23.3	9.4				66.6
$4a_{1g}$	−6.32	66.5			23.6		1.2	7.3
$3a_{2u}$	−9.07	13.1			6.0		6.0	68.7
$3e_u$	−9.27		4.0	29.7		1.2	5.6	48.8
$3e_g$	−9.49		2.7	35.4			4.5	33.7
$3a_{1g}$	−9.70	22.6				0.7	4.2	67.2
$2a_{2u}$	−12.52	0.4			5.6			41.0
$2e_g$	−12.52		3.0			4.0		40.6
$2a_{1g}$	−12.67	0.7					48.9	
$2e_u$	−12.73		7.0					43.9

[a] $\sigma = 4d_{z^2}$; $\pi = 4d_{yz}$; $\delta = 4d_{x^2-y^2}$. [b] Spaces indicate contributions less than 0.4%. Hydrogen 1s contributions are not listed, but are the difference between the sum of the contributions shown and 100%.

$Mo_2(NH_2)_6$. The results of the Xα–SW calculation on the model system $Mo_2(NH_2)_6$ are presented in Figure 2. The PXα results and orbital energies are listed in Table IV. It is immediately obvious that there are considerable differences in the uppermost energy levels between the alkoxide and amide calculations. These differences are caused by the lower electronegativity of the nitrogen atoms, resulting in lone-pair orbitals which are ~3 eV higher in energy than those of oxygen, and now occur in the same general region as the Mo–Mo π and σ levels. The NH_2 groups were oriented parallel to the Mo–Mo bond, placing the nitrogen lone-pair orbitals perpendicular to the Mo–Mo and Mo–N axes. These lone-pair orbitals span the same representations as the noninteracting oxygen lone pairs: a_{2g}, a_{1u}, e_u, and e_g. The two highest filled MO's are the $1a_{1g}$ and $1a_{1u}$ lone-pair orbitals which are 100% nitrogen 2 p in character. The other two lone-pair levels ($4e_u$ and $4e_g$), however, are involved in Mo–N π bonding. The $4e_g$ MO has 15% Mo character while $4e_u$ has 33%. The greater amount of metal mixing, relative to $Mo_2(OH)_6$ where there was only a 3% Mo contribution in the $4e_g$ and $4e_u$ orbitals, is probably due to the smaller energetic separation of the nitrogen lone pairs and the molybdenum d orbitals, allowing increased metal–ligand interactions.

The LCAO projection emphasizes some other interesting features of the Mo–N bonding in these levels. The first is the proportionately large amount of δ character mixed into the $4e_g$ orbital, improving the Mo–N bonding and reducing the Mo–Mo π^* character of the orbital. The other feature is a small, but definite, Mo–N σ^*-antibonding interaction present in both of the MO's. Thus, while there is a larger Mo–N π-bonding contribution in $Mo_2(NH_2)_6$ as compared to $Mo_2(OH)_6$, the commensurate increase in σ^* mixing tends to cancel much, if not all, of the additional Mo–N π bonding, making the Mo–L bonding in $Mo_2(NH_2)_6$ and $Mo_2(OH)_6$ quite similar.

The principal metal–metal bonding MO's, as with $Mo_2(OH)_6$, are the $5e_u$ (π) and $4a_{1g}$ (σ) levels. The $5e_u$ orbital is shown in Figure 7. In contrast to $Mo_2(OH)_6$, the $5e_u$ orbital in $Mo_2(NH_2)_6$ has no δ^* AO character. The smaller Mo contribution in the $5e_u$ level relative to that in the alkoxide is due to the increased metal–ligand interaction which partitions the Mo–Mo π-bonding character between the $5e_u$ and $4e_u$ orbitals. The $4a_{1g}$ orbital, by contrast, has a greater Mo contribution, most of which comes from increased metal 5s orbital character.

The metal–ligand σ-bonding orbitals in $Mo_2(NH_2)_6$ are analogous to those discussed for $Mo_2(OH)_6$. The only important difference is that a small amount of Mo π and π^* character is present in the $3e_u$ and $3e_g$ MO's. This π mixing has a slight destabilizing effect which raises the energy of the $3e_g$ and $3e_u$ orbitals relative to that of the $3a_{2u}$ and $3a_{1g}$ MO's. There is also

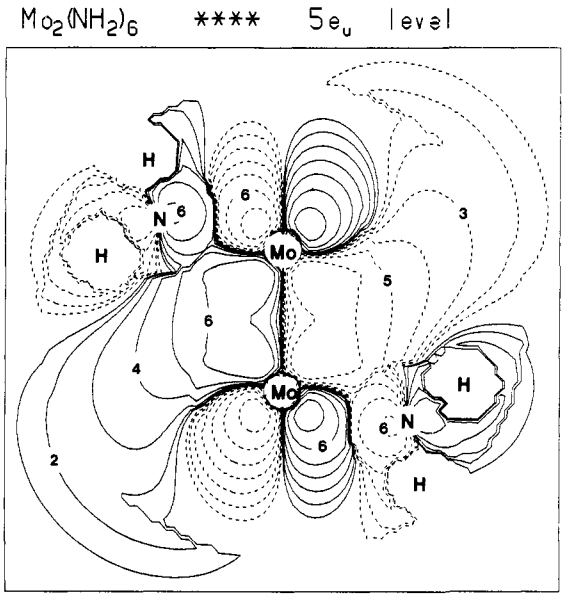

Figure 7. Contour plot of the $5e_u$ orbital of $Mo_2(NH_2)_6$.

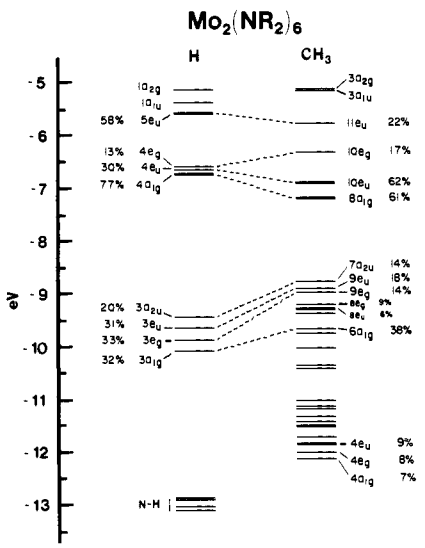

Figure 8. Xα–SW energy level diagrams for $Mo_2(NH_2)_6$ and $Mo_2(NMe_2)_6$. Only the occupied upper valence orbitals are shown. Percent characters refer to the atomic-sphere molybdenum contributions to that orbital and are only listed for levels with 5% or more Mo character.

increased nitrogen σ donation into the molybdenum δ levels as compared to the case for $Mo_2(OH)_6$. Qualitatively, this would be anticipated because of the lower electronegativity of the nitrogen atoms. The N–H bonding levels receive small metal contributions by way of the M–L in-plane π bonding, but such bonding is more limited here than in $Mo_2(OH)_6$ and contributes little to the total M–L bonding.

$Mo_2(NMe_2)_6$. While substituting a hydrogen for a large alkyl group considerably reduces the complexity of the calculation, it might be objected that the saving of money is at the cost of details important to the description of the electronic structure of the "real" molecule. This objection has been addressed by performing a calculation on $Mo_2(NMe_2)_6$. The results of the Xα calculations are presented in Figure 8. As an LCAO projection would have been prohibitively expensive on such a large system (56 atoms), only the atomic-sphere charge contributions for $Mo_2(NMe_2)_6$ and $Mo_2(NH_2)_6$ will be compared and discussed in this section.

The major difference in the upper band of valence orbitals between $Mo_2(NMe_2)_6$ and $Mo_2(NH_2)_6$ is the shifting of metal density from the 11 e_u level down into the $10e_u$, which becomes the principal Mo–Mo π-bonding orbital. A comparison of the contour plots of the $5e_u$ MO of $Mo_2(NH_2)_6$ (Figure 7) with the

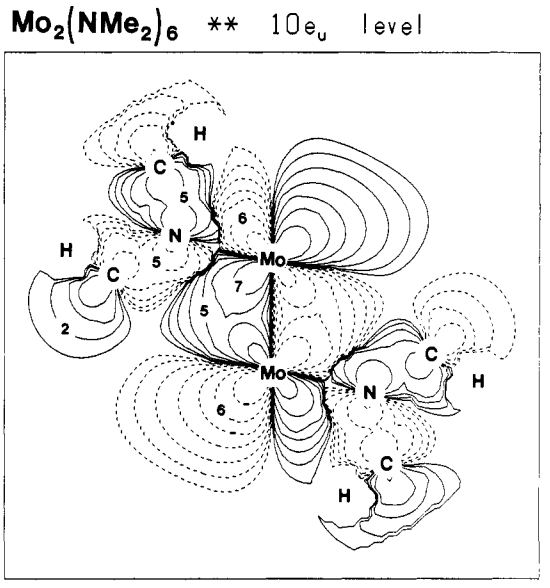

Figure 9. Contour plot of the $10e_u$ orbital of $Mo_2(NMe_2)_6$.

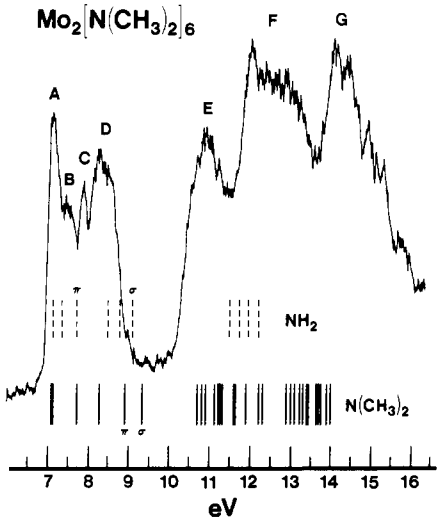

Figure 10. He I PES of $Mo_2(NMe_2)_6$ along with the calculated IP's for $Mo_2(NH_2)_6$ and $Mo_2(NMe_2)_6$. The calculated IP's have been shifted to match the first calculated and experimental peaks.

$10e_u$ MO of $Mo_2(NMe_2)_6$ (Figure 9) shows that the relative orbital characters are quite similar, the main difference lying in the Mo–N interactions. Despite this shift of metal density, the overall Mo–Mo and Mo–N bonding is very comparable in the two cases. The Mo–N σ-bonding nature of the lower orbitals is also similar, although it is now distributed over several more orbitals. For example, in $Mo_2(NH_2)_6$ the e_u contribution to the M–L σ bonding was concentrated in the $3e_u$ MO (33% Mo), while in $Mo_2(NMe_2)_6$ it is spread over the $9e_u$ (18% Mo), $8e_u$ (6%), $6e_u$ (3%), $5e_u$ (5%), and $4e_u$ (9%) levels, some of which have Mo–N in-plane π bonding mixed in as well. This occurs also for the Mo–Mo σ-bonding a_{1g} levels, with the difference in molybdenum contributions between the $4a_{1g}$ orbital in $Mo_2(NH_2)_6$ and the $8a_{1g}$ level in $Mo_2(NMe_2)_6$ spread out over the various lower a_{1g} orbitals in the dimethylamide calculation. This greater mixing is due to the carbon atoms on the nitrogen atoms which, through a greater variety of different N–C bonding interactions, cause more mixing of the various orbital characters. This has no significant effect on the bonding, except to make it less easy to interpret than in the simple model systems.

The 6–20-eV He I and He II photoelectron spectra of $Mo_2(NMe_2)_6$ are shown in Figure 5c,d. In Figure 10, the low-energy portion of the He I spectrum is compared to the calculated IP's for $Mo_2(NH_2)_6$ and $Mo_2(NMe_2)_6$ which have each been shifted to match the first calculated IP with the first experimental peak value. The calculated IP's are also listed in Table II for Mo_2-

Table V. Calculated Transition-State Ionization Potentials for $Mo_2[N(CH_3)_2]_6$

level	IP[a]	level	IP
$3a_{2u}$	6.98	$7e_u$	(11.8)
$3a_{1u}$	(7.0)	$7e_g$	12.11
$11e_u$	7.63	$2a_{1u}$	(12.2)
$10e_g$	8.15	$1a_{2g}$	(12.8)
$10e_u$	(8.8)	$6e_g$	(12.9)
$8a_{1g}$	9.23	$5a_{2u}$	12.98
$7a_{2u}$	(10.6)	$6e_u$	(13.1)
$9e_u$	(10.7)	$5a_{1g}$	(13.2)
$9e_g$	10.81	$5e_g$	(13.3)
$8e_g$	(11.0)	$5e_u$	(13.3)
$8e_u$	(11.1)	$1a_{1u}$	13.54
$6a_{2u}$	(11.1)	$4a_{2u}$	(13.6)
$7a_{1g}$	11.19	$4e_u$	(13.6)
$6a_{1g}$	(11.5)	$4e_g$	(13.8)
$2a_{2g}$	(11.5)	$4a_{1g}$	13.90

[a] Energies in eV. Values in parentheses are estimates from nearby ionizations and should be accurate to within 0.1 eV.

Table VI. Experimental Ionization Potentials for $Mo_2(NMe_2)_6$

peak	IP[a]	peak	IP[a]
A	6.74	E	10.72
B	7.11	F	11.9
C	7.49		12.48
D	7.98	G	14.28

[a] Energies in eV.

$(NH_2)_6$ and Table V for $Mo_2(NMe_2)_6$. The experimental peak energies are given in Table VI. The upper valence region for $Mo_2(NMe_2)_6$ in the PES is clearly more complicated than that observed for $Mo_2(OCH_2CMe_3)_6$. The calculations predict that peak A arises from the noninteracting a_{2g} and a_{1u} nitrogen lone pairs which are nearly degenerate in energy. The sharpness of the ionization band, characteristic of lone-pair ionizations, supports this assignment. Peaks B and C are assigned to the $11e_u$ and $10e_g$ orbitals which are primarily nitrogen lone pair. The $11e_u$ orbital is Mo–N antibonding but is stabilized in turn by the Mo–Mo π-bonding interaction, while the $10e_g$ orbital has exactly the opposite characters, viz., Mo–N bonding and Mo–Mo π^* antibonding. As was the case for the $4e_g$ MO of $Mo_2(NH_2)_6$, the mixing of Mo δ orbitals with the π^* levels will reduce the Mo–Mo π^* interactions in the $10e_g$ orbital as well as improve the Mo–N bonding. The broad, multiple peak D arises from the Mo–Mo π ($10e_u$) and σ ($8a_{1g}$) MO's which are too close in energy to be resolved. Support for this assignment comes from the He II PES which shows peak D increasing in intensity relative to A, B, and C. This indicates a considerably higher molybdenum contribution to peak D, completely consistent with the proposed level orderings from the $Mo_2(NMe_2)_6$ calculation. While the energy spread of the calculated IP's is a bit too great for the upper valence region, the levels are too compressed for the higher energy region of the PES. Some assignments, however, can be hazarded despite the presence of a good deal of mixing in these lower orbitals. Peak E probably results from ionizations from the Mo–N bonding $7a_{2u}$, $9e_u$, and $9e_g$ orbitals, with region F arising principally from C–H bonding levels and peak G from the N–C bonding orbitals, consistent with their relative decreases in intensity in the He II spectrum.

We conclude, therefore, that although there are differences between the Xα–SW calculations on $Mo_2(NH_2)_6$ and $Mo_2(NMe_2)_6$, the use of NH_2, OH, and CH_3 groups in place of the larger ligand systems should allow a fundamentally correct description of the electronic structures and bonding interactions in the real compounds.

$Mo_2(CH_3)_6$. The Xα–SW results for the calculation on $Mo_2(CH_3)_6$ are shown in Figure 2. The PXα orbital characters and orbital energies are listed in Table VII. One might naively expect that the electronic structure of $Mo_2(CH_3)_6$ to be the simplest of the series as there are no lone-pair orbitals or M–L

Table VII. Energies and Percent Characters of the Highest Occupied Orbitals of $Mo_2(CH_3)_6$

		Mulliken percent contributions						
		Mo[a,b]					C	
level	ϵ, eV	σ	π	δ	5s	5p	2s	2p
$5e_u$	−4.27		46.3	27.8		6.8	5.0	14.1
$3a_{2u}$	−4.77	14.3			20.0		10.6	55.1
$4e_u$	−5.04		43.6	24.1		2.4	5.6	24.0
$4a_{1g}$	−5.06	9.1			23.8		9.5	57.3
$4e_g$	−5.30		3.2	56.4		9.8	7.5	23.1
$3a_{1g}$	−6.72	76.8					2.1	20.4
$1a_{2g}$	−8.86							34.9
$3e_g$	−8.88		1.6					24.3
$2a_{2u}$	−8.93							20.2
$3e_u$	−9.11		3.6	1.2				19.3
$1a_{1u}$	−9.27							33.8
$2a_{1g}$	−9.37	3.0						22.3
$2e_u$	−9.46		4.6					18.2
$2e_g$	−9.57		1.2	4.1				21.5

[a] $\sigma = 4d_{z^2}$; $\pi = 4d_{xz}, 4d_{yz}$; $\delta = 4d_{xy}, 4d_{x^2-y^2}$. [b] Spaces indicate contributions less than 0.4%. Hydrogen 1s contributions are not listed, but are the difference between the sum of the contributions shown and 100%.

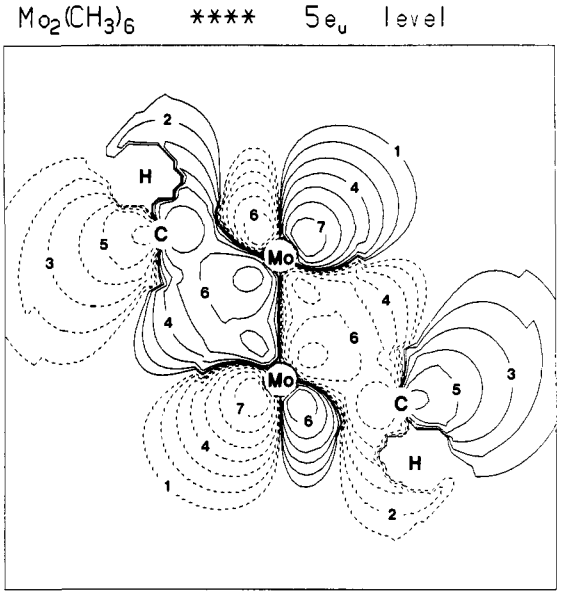

Figure 11. Contour plot of the $5e_u$ orbital of $Mo_2(CH_3)_6$.

π-bonding interactions to complicate the PES or the interpretation of the bonding. On the contrary, the electronic structure of $Mo_2(CH_3)_6$ turns out to be rather complex and extremely interesting.

The HOMO is the $5e_u$ orbital (Figure 11), which while primarily Mo–Mo π bonding, has substantial δ^* character which weakens the bonding in this orbital. The δ^* mixing, however, serves to reduce the Mo–C antibonding interaction by hybridizing the molybdenum π orbitals away from the carbon atoms and introducing an in-plane "π"-type bond between the carbon atoms and molybdenum atoms. As a result, the Mo–C interaction in the $5e_u$ level is only weakly antibonding or perhaps even nonbonding.

The next level is the $3a_{2u}$, which, in analogy with the other M_2L_6 systems examined here, is Mo–C σ bonding and Mo–Mo σ^* antibonding. The orbital has contributions from both $4d_{z^2}$ (14%) and 5s (20%) in which the s/d_{z^2} mixing is such as to strengthen the Mo–C bonding and reduce the Mo–Mo σ^* character. The $4e_u$ orbital is similar in composition to the $5e_u$ orbital, but it is Mo–C bonding rather than nonbonding. The π–δ^* hybridization in the $4e_u$ orbital is different from that in the $5e_u$ orbital, as is apparent by comparison of the orbital contour plots (Figures 11 and 12). By comparison, in $Mo_2(OH_6)$ there was one e_u level (the $5e_u$) which was practically pure Mo–Mo π bonding mixed

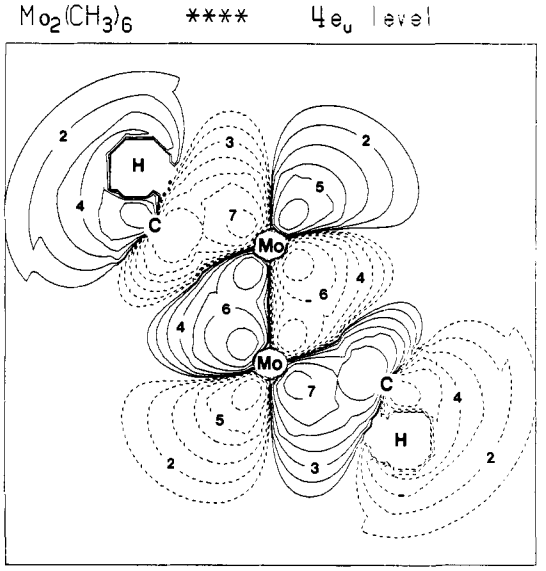

Figure 12. Contour plot of the $4e_u$ orbital of $Mo_2(CH_3)_6$.

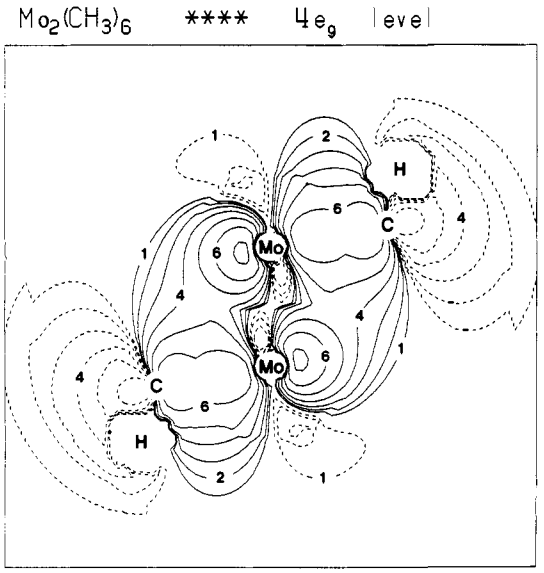

Figure 13. Contour plot of the $4e_g$ orbital of $Mo_2(CH_3)_6$.

with Mo–O π^* and σ^* characters, while the other e_u orbital (the $3e_u$) was Mo–O σ bonding via molybdenum δ-type AO's. $Mo_2(CH_3)_6$, however, has much stronger ligand σ donation which causes these two types of orbital to blend together forming two new e_u levels of similar δ and π characters. Thus, although the Mo–Mo π bonding is weakened by the δ^* character introduced, the driving force for the hybridization appears to be the strong Mo–C interactions and the minimization of the M–L σ^* antiboding in the $5e_u$ MO.

In each of the previous calculations the Mo–Mo σ bond was divided between the $3a_{1g}$ and $4a_{1g}$ MO's, but with the latter possessing most of the metal character and therefore contributing most to the Mo–Mo σ bonding. The situation in $Mo_2(CH_3)_6$, however, is considerably different. The $4a_{1g}$ orbital has only a 33% contribution from the Mo atoms, and it is mostly 5s in character (9% $4d_{z^2}$, 24% 5s). The d_{z^2}/s mixing has increased to the point that the Mo–C antibonding interaction in the $4a_{1g}$ orbital is drastically reduced. Indeed, the Mulliken overlap population between each Mo and C atom in this orbital is +0.037, indicating a bonding, rather than antibonding, interaction. The $4e_g$ MO (Figure 13) exemplifies the strong Mo–C bonding and large ligand σ donation onto the molybdenum atoms. The $4e_g$ level is composed of 56% δ, 10% 5p, and 3% π^* Mo contributions, and since all these metal orbitals are formally unoccupied, the methyl groups are donating almost 70% of the electron density originally localized

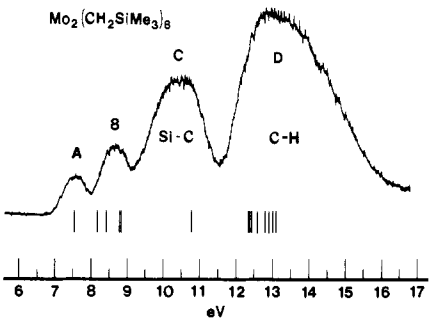

Figure 14. He I PES of $Mo_2(CH_2SiMe_3)_6$ along with the calculated IP's for $Mo_2(CH_3)_6$. The calculated values have been shifted to match the first calculated and experimental peaks.

on them into the molybdenum orbitals. A comparison of this with the 29% Mo contribution in the related $3e_g$ orbital in $Mo_2(OH)_6$ emphasizes the much greater amount of M–L σ donation occurring in $Mo_2(CH_3)_6$. The last orbital involved in substantial Mo–Mo and Mo–C bonding is the $3a_{1g}$ MO which has most of the Mo–Mo d_{z^2} σ-bonding character, and although there is a fairly strong Mo–C bonding contribution, the principal function of the $3a_{1g}$ level is Mo–Mo σ bonding. The orbitals below the $3a_{1g}$ are almost completely involved in C–H bonding.

The 6–20-eV He I and He II PE spectra of $Mo_2(CH_2SiMe_3)_6$ are shown in Figure 5e,f. The calculated ionization potentials for $Mo_2(CH_3)_6$ are listed in Table II. In Figure 14 the low-energy region of the He I spectrum is compared to the calculated IP's which have been shifted to match the first calculated peak with the first experimental peak. Peaks D and C can be unambiguously assigned to the ionization of C–H and Si–C bonding levels,[31] respectively. Assignment of peaks A and B is mainly a question of where to place the $3a_{2u}$ level, since the calculation places it in the valley between A and B. We begin with the assumption that band B is composed, at least in part, of the Mo–C orbitals ($4e_g$ and $4e_u$), an assumption that is supported by the calculation, the He I vs. He II intensities, and an interpretation of the PES of $Cr(CH_2SiMe_3)_4$.[31] The following straightforward argument then allows us to place the $3a_{2u}$ and $3a_{1g}$ ionizations. In the absence of metal–metal bonding, the Mo–C bond via the Mo d_{z^2} orbital should be of comparable energy with the δ (d_{xy}, $d_{x^2-y^2}$) set of AO's. The effect of Mo–Mo bonding is the formation of two new d_{z^2}–C bonding combinations, one stabilized by the Mo–Mo bonding (the $3a_{1g}$ level) and the other destabilized by the Mo–Mo σ^*-antibonding interaction (the $3a_{2u}$). By invoking Mo 5s mixing, the σ^*-antibonding interaction can be reduced somewhat. We feel that this analysis, although admittedly oversimplified, can be used to rationalize the placement of the $3a_{2u}$ orbital under peak A and the $3a_{1g}$ orbital under peak C. Peak A is, therefore, most likely composed of ionizations from the $5e_u$ Mo–Mo π-bonding and $3a_{2u}$ Mo–C σ-bonding (Mo–Mo σ^*) orbitals. Band B then arises from the secondary Mo–Mo and Mo–C σ-bonding $4a_{1g}$ orbital, along with the Mo–C σ-bonding $4e_g$ and $4e_u$ orbitals. The He I intensity ratio for peak A to B is 1:2.3, while the He II intensity ratio is 1:1.5. Summing up only the Mo 4d contributions in the levels assigned for peaks A and B, we obtained an A:B ratio of 1:1.6. Since the He II intensities reflect to a greater degree the metal contributions present, we consider the proposed assignments consistent with the He I/He II intensity ratios as well as the overall structure of the PES. The rather unprecedented assignment and positioning of the $3a_{1g}$ MO, as the main component of the Mo–Mo σ bond, will later be shown to be quite reasonable in light of the comparative chemistry and properties of these M_2L_6 compounds.

Ligand Effects on the Reactivity and Structure of Mo_2L_6 Compounds. The detailed nature of the orbital characters and bonding in each of the separate Mo_2L_6 model systems has been discussed in the previous sections. We will now compare the three systems in order to assess whether or not these theoretical models

(31) Evans, S.; Green, J. C.; Jackson, S. E. *J. Chem. Soc., Faraday Trans. 2* **1973**, 191.

Table VIII. Molybdenum Orbital Mulliken Populations[a, b]

compd	σ	π	δ	5s	5p	Mo charge
$Mo_2(OH)_6$	1.035	2.168	1.443	0.279	−0.354	1.429+
$Mo_2(NH_2)_6$	1.030	2.204	1.659	0.289	−0.337	1.155+
$Mo_2(CH_3)_6$	1.044	2.101	2.315	0.516	−0.589	0.614+

[a] $\sigma = 4d_{z^2}$; $\pi = 4d_{xz}, 4d_{yz}$; $\delta = 4d_{xy}, 4d_{x^2-y^2}$; $5p = 5p_x, 5p_y, 5p_z$. [b] For one Mo atom.

can give us a better perspective on the origins of the various physical properties and reaction chemistries of the real compounds.

The Mulliken populations[32] and resultant metal charges from the LCAO projections are presented in Table VIII. The negative 5p populations are an artifact of the Mulliken analysis on diffuse orbitals.[33] Although the σ and π orbitals retain essentially the same occupancies in the three compounds, the δ (and, to a lesser extent, the 5s) AO's show a dramatic increase in their populations particularly from the amide to the methyl compound. The molybdenum atomic charge drops from 1.429+ in $Mo_2(OH)_6$, to 1.155+ for $Mo_2(NH_2)_6$, and finally to 0.614+ in $Mo_2(CH_3)_6$. This general trend arises from the decreasing electronegativities of the oxygen, nitrogen, and carbon atoms which favor an increased donation of electron density to the molybdenum atoms. The principal mechanism for transferring charge from the ligands to the metals is through the Mo–L σ bonds. As a crude first approximation, it is not unreasonable to assume that the strength of the M–L bond can be related to the occupation of the δ (d_{xy}, $d_{x^2-y^2}$) metal orbitals, which in the extreme of no metal–ligand bonding would be unoccupied. Two other important factors must also be considered, namely, the extent of Mo–L π bonding and the mixing of Mo–L π^* or σ^* character in the occupied MO's. $Mo_2(OH)_6$ and $Mo_2(NH_2)_6$ both have Mo–L π bonding, and although $Mo_2(NH_2)_6$ has more Mo–N π-bonding orbitals with higher metal contributions, there is Mo–N σ^* character mixed into each of the upper e_g and e_u Mo–N π-bonding levels. The σ^* character most probably cancels most of the additional Mo–N π and σ bonding, so despite the larger Mo δ AO population in $Mo_2(NH_2)_6$, the metal–ligand bonding is probably similar in the amine and the alkoxide.

$Mo_2(CH_3)_6$ is, however, distinctly different from both $Mo_2(OH)_6$ and $Mo_2(NH_2)_6$. The δ population is distinctly larger, the Mo–C σ-bonding orbitals show large metal contributions, and there are no occupied orbitals with Mo–C antibonding character. That this adds up to much stronger Mo–L bonding in $Mo_2(CH_3)_6$ than in the other two systems is reflected in both the Mo–C bond lengths and reaction chemistry of $Mo_2(CH_2SiMe_3)_6$. The Mo–C bond length of 2.13 Å is among the shortest known Mo–C (alkyl) bond lengths. An interesting and illustrative comparison is the quadruply bonded complex $[Mo_2(CH_3)_8]^{4-}$ which has a Mo–C bond length of 2.29 (1) Å (mean) and a Mo–Mo distance of 2.148 (2) Å.[34] The methyl groups in $Mo_2(CH_3)_6$ have a Mulliken charge of 0.2–, implying that each CH_3^- group has donated 0.8 electrons onto the molybdenum atoms. A similar σ donation in $[Mo_2(CH_3)_8]^{4-}$ would transfer 3.18 electrons to each of the Mo atoms. Since each Mo $d_{x^2-y^2}$ orbital (the d_{xy} orbital is occupied and is involved in M–M δ bonding) can only accept 2.0 electrons from M–L bonding, there must subsequently be less M–L σ donation and weaker covalent bonding. Thus, the depopulation of the d_{xy} orbitals in making the d^3–d^3 triply bonded compound facilitates stronger Mo–C bonding at the expense of some Mo–Mo bonding.

The prediction of stronger Mo–L bonding in the alkyl complex as compared to the alkoxide or amido complexes is consistent with the reactivity of the Mo_2L_6 compounds. Carbon dioxide is known to insert into the M–L bonds of a number of Mo_2L_6 and W_2L_6 compounds:

$$Mo_2(OR)_6 + 2CO_2 \rightleftarrows Mo_2(OR)_4(O_2COR)_2 \quad (1)^{12}$$

$$W_2(OR)_6 + 2CO_2 \rightleftarrows W_2(OR)_4(O_2COR)_2 \quad (2)^{35}$$

$$Mo_2(NR_2)_6 + 4CO_2 \rightarrow Mo_2(NR_2)_2(O_2CNR_2)_4 \quad (3)^{36}$$

$$W_2(NR_2)_6 + 6CO_2 \rightarrow W_2(O_2CNR_2)_6 \quad (4)^{11}$$

$$W_2Me_2(NR_2)_4 + 4CO_2 \rightarrow W_2Me_2(O_2CNR_2)_4 \quad (5)^{11}$$

$$M_2(CH_2R)_6 + CO_2 \rightarrow \text{no reaction (M = Mo, W)} \quad (6)^2$$

Reactions 1 and 2 are reversible and have been proposed to proceed by direct attack on the M–OR bond. Reactions 4 and 5 are irreversible and occur via an amine-catalyzed mechanism:[11]

$$R_2NH + CO_2 \rightleftarrows R_2NCOOH$$

$$M\text{–}NR_2 + R_2NCOOH \rightarrow M\text{–}O_2CNR_2 + HNR_2 \quad (7)$$

Although the mechanistic studies of the insertion of CO_2 into Mo–NR_2 bonds (reaction 3) have not been completed, it is reasonable to assume that a similar route is taken. The amido compounds also undergo a number of metathetic reactions in which $M_2(NR_2)_{6-n}Y_n$ (Y = Cl, Br, I, Me, Et, *n*-butyl, and CH_2SiMe_3)[9,13,14,25,37] species may be prepared, as can the alkoxide compound, $Mo_2(OR)_6$, by the reaction of $Mo_2(NR_2)_6$ with alcohols and trialkylsilanols.[25]

In light of the reactivity of the alkoxy and amido species, the fact that $Mo_2(CH_2R)_6$ or $W_2(CH_2R)_6$ compounds do not react at all with CO_2, COS, or CS_2 is most interesting, as is the apparent lack of substitution reactions. We feel that the limited reactivity of the M–C bonds in $M_2(CH_2R)_6$ compounds is a consequence of the stronger, more covalent M–C bonding. Further evidence emphasizing the electronic differences between $Mo_2(OR)_6$ and $Mo_2(CH_2R)_6$ comes from the Lewis base addition chemistries of the two. $Mo_2(OR)_6$ (R = $SiMe_3$, CH_2CMe_3) readily adds Lewis base ligands[25] such as amines and phosphines to form $Mo_2(OR)_6L_2$ adducts whereas $Mo_2(CH_2SiMe_3)_6$ does not.[38] While it has been proposed that the differences in reactivities between the alkoxide and alkyl M_2L_6 compounds is most likely caused by electronic factors, no specific arguments have been advanced. According to the calculations the considerably larger σ donation from the alkyl groups has reduced the positive charge on the Mo atoms to the point where the coordination of an electron-donating Lewis base is undesirable. Conversely, the higher positive charge present on the metal atoms in the alkoxides implies an electron deficient condition relative to the alkyl, which places the addition and insertion that $Mo_2(OR)_6$ compounds are noted for into the proper electronic perspective. $Mo_2(NR_2)_6$ lies somewhere between the electronic extremes represented by $Mo_2(OR)_6$ and $Mo_2(CH_3)_6$, and since the chemistry of the amido complexes is dominated to a much greater degree by steric effects and amine-catalyzed reactions, it is more difficult to sort out the electronic factors and compare them with the calculations.

Ligand electronic factors are also important to the metal–metal bonding. That there is an effect can be seen by comparing the Mo–Mo bond distances in $Mo_2(OCH_2CMe_3)_6$ (2.222 (2) Å), $Mo_2(NMe_2)_6$ (2.214 (3) Å), and $Mo_2(CH_2SiMe_3)_6$ (2.167 (?) Å). Once again the alkyl compound stands out as substantially different from the alkoxide and amide species. The ligand-based electronic effects on the metal–metal bonding can be separated into three general categories: (1) ligand donation into M–M antibonding orbitals, (2) ligand donation into the formally unoccupied metal s and p orbitals, and (3) the stabilization of M–M bonding levels by ligand interactions.

The donation of electron density into metal–metal antibonding orbitals will naturally have a destabilizing influence on the M–M bonding. In Mo_2L_6 systems, donations into the metal e_g (π^*) and a_{2u} (σ^*) orbital combinations are expected to be the main contributors to the weakening of the Mo–Mo bond. The sum of the

(32) Mulliken, R. S. *J. Chem. Phys.* **1955**, *23*, 1833.
(33) Ammeter, J. H.; Bürgi, H.-B.; Thibeault, J. C.; Hoffmann, R. *J. Am. Chem. Soc.* **1978**, *100*, 3686.
(34) Cotton, F. A.; Troup, J. M.; Webb, T. R.; Williamson, D. H.; Wilkinson, G. *J. Am. Chem. Soc.* **1974**, *96*, 3824.
(35) Chisholm, M. H.; Extine, M. *J. Am. Chem. Soc.* **1975**, *97*, 5625.
(36) Chisholm, M. H.; Reichert, W. W. *Inorg. Chem.* **1978**, *17*, 767.
(37) Chisholm, M. H.; Cotton, F. A.; Extine, M. W.; Murillo, C. A. *Inorg. Chem.* **1978**, *17*, 2338.
(38) Chisholm, M. H., personal communication.

π^* metal contributions in all the occupied valence e_g orbitals shows that there is 6% π^* character in $Mo_2(CH_3)_6$, 12% in $Mo_2(NH_2)_6$, and 10% in $Mo_2(OH)_6$. The higher π^* characters in the alkoxide and amide arise from Mo–L π bonding which is not possible in the alkyl compound. The effect of the Mo–Mo π^* character is fairly minor when compared to the Mo–Mo σ^* interactions introduced in the Mo–L a_{2u} orbitals, where the metal contributions vary from 28% in the alkoxide to 34% in the alkyl. The Mo–Mo antibonding interaction in the a_{2u} levels is partially offset by the second electronic factor—ligand donation into the 5s Mo AO's. The mixing of 5s character into the a_{2u} MO's is such as to hybridize with the d_{z^2} orbitals lessening the Mo–Mo σ^* interaction and maximizing the Mo–L bonding. It is notable that the Mo–Mo σ^* character in $Mo_2(OH)_6$ is split between the $3a_{2u}$ and $2a_{2u}$ orbitals, with the $3a_{2u}$ having pure d_{z^2} character and the $2a_{2u}$ pure 5s. This invalidates the d_{z^2}/s hybrid stabilization argument for $Mo_2(OH)_6$ since there is no d_{z^2}–s mixing, but, on the basis of the $Mo_2(NMe_2)_6$ calculation where much more orbital mixing occurs, this is probably just a "model system" artifact induced by the low energy of the O–H bonding levels. Despite the greater ligand donation in the $3a_{2u}$ orbital in the $Mo_2(CH_3)_6$ calculation, the corresponding increase in the Mo 5s mixing may actually reduce the metal–metal π^*-antibonding interaction relative to the amide and alkoxide complexes.

There is also 5s mixing in the $4a_{1g}$ Mo–Mo σ-bonding levels. The 5s mixing contributes to the Mo–Mo bonding and reduces the Mo–L antibonding character. This is especially true for $Mo_2(CH_3)_6$ where, instead of the Mo–L antibonding interactions seen in the $4a_{1g}$ MO's for $Mo_2(OH)_6$ and $Mo_2(NH_2)_6$, there is now Mo–C bonding. This results from a dramatically increased 5s to $4d_{z^2}$ hybridization ratio caused, in part, by the greater amount of alkyl σ donation to the Mo atoms. There is also some ligand donation into the Mo $p_{x,y}$ orbitals but this should have little or no effect on the metal–metal bonding since both the π and π^*p AO combinations are roughly equally occupied, yielding no net contribution to the Mo–Mo π bonding.

The last major factor affecting the Mo–Mo bonding is, in many ways, the most important. The Mo–Mo σ-bonding a_{1g} orbital can mix with the ligand a_{1g} combination of orbitals directed at the metal atoms to form two new a_{1g} orbitals. Both are still Mo–Mo bonding in character, but the lower energy orbital is Mo–L bonding while the upper is Mo–L antibonding. If the "free" ligand a_{1g} level is lower in energy than the "free" metal–metal bonding a_{1g} orbital, when the two interact most of the metal character will be pushed up into the upper a_{1g} MO which is Mo–L antibonding while the lower Mo–L bonding a_{1g} level will have mostly ligand character. This, we believe, is what happens in both $Mo_2(OR)_6$ and $Mo_2(NH_2)_6$. Conversely, when the ligand levels are above the metal–metal bonding a_{1g} orbital, as in $Mo_2(CH_3)_6$, the metal character is mainly concentrated in the Mo–L bonding MO, explaining the switch in the $3a_{1g}$ and $4a_{1g}$ Mo orbital contributions relative to the other two cases. Similar situations have been observed in the Xα calculations on $M_2(O_2CH)_4$ (M = Cr, Mo)[39,40] and $[M_2Cl_8]^{n-}$ (M = Mo, Re).[41,42] The shift of the metal density into a lower orbital stabilizes the M–M σ bonding but at the expense of the ligand a_{1g} orbital. We believe that this, along with the increased Mo 5s contributions, is the principal reason for the shorter M–M bond lengths in the $M_2(CH_2SiMe_3)_6$ (M = Mo, W) compounds relative to the alkoxide or amide systems.

The lowest unoccupied molecular orbital (LUMO) in each calculation is an e_g Mo–Mo π^* orbital. The HOMO–LUMO energy gap is quite large, around 3 eV ($\sim$24 000 cm^{-1}), which agrees well with the experimental observation that electronic transitions all occur in the UV but tail into the visible, accounting for the characteristic yellow color of these M_2L_6 compounds. It has been observed, however, that the products of ligand addition reactions with $Mo_2(OR)_6$ compounds have intense red or purple colors.[25] These $Mo_2(OR)_6L_2$ derivatives have four terminally bonded ligands to each Mo atom forming a staggered $L_4M{\equiv}ML_4$ triply bonded structure.[13] The change in ligand coordination from three to four breaks the threefold symmetry and attendant degeneracy of the $d_{x^2-y^2}$ with the d_{xy} orbital. The $d_{x^2-y^2}$ AO's continue to participate in Mo–L bonding, but the d_{xy} orbitals, which are less destabilized by ligand donation, rise in energy to become low-lying Mo–Mo δ and δ^* virtual orbitals, thus facilitating lower energy optical transitions. In the reaction of $Mo_2(NMe_2)_6$ with CO_2 the product formed is $Mo_2(O_2CNMe_2)_4(NMe_2)_2$ which has two bridging O_2CNMe_2 units, two chelating O_2CNMe_2 ligands (one on each Mo), and two terminal NMe_2 ligands (one on each Mo) forming a L_5M ML_5 type triple bond.[35] The presence of an approximate fivefold axis, as well as the similar donor properties of oxygen and nitrogen, will, to a larger degree, preserve the degeneracy d_{xy} and $d_{x^2-y^2}$ AO's. Thus the Mo–Mo π^* orbital is, once again, expected to be the LUMO. The pale yellow color of this compound is consistent with this symmetry analysis which offers, we believe, an interesting structural/electronic transition relationship for d^3–d^3 triply bonded compounds.

Finally, we will address the question of rotational conformer preference in M_2L_6 compounds. Hoffmann and Albright[19] have recently suggested that the M_2L_6 compounds are staggered only because of steric interactions between the bulky ligands; if this factor could be eliminated, they argue, the molecules would prefer an eclipsed conformation. The argument is based on the possible π and δ hybridizations under the two symmetries involved, staggered (D_{3d}) and eclipsed (D_{3h}). In the staggered geometry the M–M π-bonding orbital has e_u symmetry, in which only the δ^* can hybridize with the π orbital. In the eclipsed geometry, by contrast, the allowed hybridization is between the π and δ metal–metal interactions in orbitals of e′ symmetry. It was argued that the δ^* hybridization in the staggered mode will weaken the metal–metal π bonding relative to the π–δ mixing in the eclipsed geometry. Thus, if there is substantial δ–π mixing, there will be an electronic rotational preference for the eclipsed ligand configuration.

Inherent in this argument are two postulates which must be questioned. The first is the assumption of strong mixing between the π and δ or δ^* sets of metal orbitals, resulting in directed hybrids. PXα results in Tables I, IV, and VII indicate that this is the case only for the methyl calculation. Thus, it is apparent that strong ligand donation is necessary to break the $D_{\infty h}$ local symmetry of the M≡M unit. The second debatable assumption is the transferability of octahedrally based ML_3 frontier orbitals to the molecular orbitals of M_2L_6. This assumption would lead to a M–M–L bond angle of 125.3°, far greater than the crystallographically observed values of 100–104°. Thus, the geometry of each ML_3 fragment is more nearly planar than octahedral, leading, we believe, to far less hybridization than was assumed by Hoffmann and Albright. Furthermore, it seems quite probable that the "bending back" of the ligands is primarily due to ligand–ligand repulsion. Therefore in the hypothetical limit of ligands, small enough to have no repulsive interactions among themselves, it seems reasonable to predict a staggered arrangement of two nearly planar ML_3 units, rather than an eclipsed conformation with markedly bent-back ligands.

Acknowledgments. We are grateful to the National Science Foundation for financial support and Professor M. H. Chisholm for supplying several samples. B.E.B. was the holder of an NSF National Needs Postdoctoral Fellowship, 1978–1979. We thank Professor M. B. Hall for helpful discussions of the photoelectron spectra.

(39) Norman, J. G., Jr.; Kolari, H. J.; Gray, H. B.; Trogler, W. C. *Inorg. Chem.* **1977**, *16*, 987.
(40) Cotton, F. A.; Stanley, G. G. *Inorg. Chem.* **1977**, *16*, 2668.
(41) Norman, J. G.; Kolari, H. J. *J. Am. Chem. Soc.* **1975**, *97*, 33.
(42) Mortola, A. P.; Moskowitz, J. W.; Rösch, N.; Cowman, C. D.; Gray, H. B. *Chem. Phys. Lett.* **1975**, *32*, 283.